



Article

# Synthesis, Structural Characterization, and Biological Activities of Organically Templated Cobalt Phosphite $(C_4N_2H_{14})[Co(H_2PO_3)_4] \cdot 2H_2O$

Najlaa Hamdi <sup>1</sup>, Souad Chaouch <sup>1</sup>, Ivan da Silva <sup>2</sup> , Mohamed Ezahri <sup>3</sup>, Mohammed Lachkar <sup>1</sup>, Rama Alhasan <sup>4</sup> , Ahmad Yaman Abdin <sup>4</sup> , Claus Jacob <sup>4</sup> and Brahim El Bali <sup>1</sup>

<sup>1</sup> Engineering Laboratory of Organometallic and Molecular Materials, Faculty of Sciences, University Sidi Mohamed Ben Abdellah, P.O. Box 1796 (Atlas), Fez 30000, Morocco

<sup>2</sup> ISIS Facility, STFC Rutherford Appleton Laboratory, Chilton, Oxfordshire OX11 0QX, UK

<sup>3</sup> Laboratoire Matériaux et Environnement, Faculté des Sciences, Université Ibn Zohr, B.P. 8106, Cité Dakhla, Agadir 80000, Morocco

<sup>4</sup> Department of Pharmacy, Building B 2.1, Room 1.13, Saarland State University, D-66123 Saarbruecken, Germany

\* Correspondence: b\_elbali@yahoo.com

Received: 17 January 2019; Accepted: 5 March 2019;

First Version Published: 12 March 2019 (doi:10.3390/sci1010013.v1);

Second Version Published: 25 July 2019 (doi:10.3390/sci1010041)



**Abstract:** A novel hybrid phosphite  $(C_4N_2H_{14})[Co(H_2PO_3)_4] \cdot 2H_2O$  was synthesized with 1,4-diaminobutane (dabn) as a structure-directing agent using slow evaporation method. Single crystal X-ray diffraction analysis showed that it crystallizes in the  $P\bar{1}$  triclinic space group, with the following unit cell parameters ( $\text{\AA}$ ,  $^\circ$ )  $a = 5.4814$  (3),  $b = 7.5515$  (4),  $c = 10.8548$  (6),  $\alpha = 88.001$  (4),  $\beta = 88.707$  (5),  $\gamma = 85.126$  (5), and  $V = 447.33$  (4)  $\text{\AA}^3$ . The crystal structure was built up from corner-sharing  $[CoO_6]$ -octahedrons, forming chains parallel to  $[001]$ , which are interconnected by  $H_2PO_3^-$  pseudo-tetrahedral units. The diprotonated 1,4-butanediammonium molecules, residing between the parallel chains, interacted with the inorganic moiety via hydrogen bonds leading thus to the formation of the 3D crystal structure. The Fourier transform infrared spectrum showed characteristic bands corresponding to the phosphite group and the organic molecule. The thermal decomposition of the compound consisted mainly of the loss of the organic moiety and the water molecules. The biological tests exhibited significant activity against *Candida albicans* and *Escherichia coli* strains in all used concentrations, while less activity was pronounced when tested against *Staphylococcus epidermidis* and *Saccharomyces cerevisiae*, while there was no activity against the nematode model *Steinernema feltiae*.

**Keywords:** hybrid phosphite; X-rays crystal structure; FTIR; thermal behavior; biological activities; antimicrobial; micro-organisms

## 1. Introduction

Hybrid organic-inorganic materials have attracted a great deal of attention in different fields because of their rich structural chemistry and wide potential applications in ion-exchange, adsorption, separation, and catalysis [1–7]. Within this class of structures, hybrid phosphite continues to attract intense research attention from all facets of material scientists since it promoted the formation of a new range of structures with various architectures and dimensionality [8]. These materials might exhibit different types: simple (single metal) [9–12], mixed-metal [13–20] or hybrid (organic-inorganic) [5,21]. In this context, we have described in the present paper the synthesis, crystal structure, spectroscopic characterization via Fourier transform infrared (FTIR) analysis, and thermal behavior of the new hybrid

phosphite  $(C_4N_2H_{14})[Co(H_2PO_3)_4] \cdot 2H_2O$ . Moreover, we have reported on the biological activities, that is, its activity against *C. albicans*, *E. coli* strains, *S. epidermidis*, and *S. cerevisiae* as a first contribution in the investigations conducted by our research group on such research in the field of phosphite materials.

## 2. Experimental

### 2.1. Synthesis

Single crystals of  $(C_4N_2H_{14})[Co(H_2PO_3)_4] \cdot 2H_2O$  were synthesized under ambient conditions. The reaction mixture of  $Co(NO_3)_2 \cdot 6H_2O$  (1 mmol, 300 mg), 1,4-diaminobutane (dabn) (2 mmol, 170 mg), and  $H_3PO_3$  (4 mmol, 300 mg) was shaken in distilled water for 6 h and then left at room temperature. After two weeks, the pink solution had concentrated and hexagonal purple crystals arised on the bottom of beker, which were harvested washed with the water-ethanol mixture (80:20) and dried in air.

### 2.2. Materials and Instrumentation

All reagents were acquired from commercial sources and used without further purification. The infrared spectrum of the compound was recorded on a VERTEX 70 FTIR Spectrometer in the range  $4000\text{--}400\text{ cm}^{-1}$  using the ATR technique at  $4\text{ cm}^{-1}$  resolution. Thermogravimetric analysis (TGA) data were recorded on an SDT-Q600 analyzer from TA Instruments (Eschborn, Germany). The temperature varied from RT to 1173 K at a heating rate of  $10^\circ/\text{min}^{-1}$ . Measurements were carried out on samples in open platinum crucibles under air flow.

### 2.3. Crystal Structure Determination

Single-crystal X-ray diffraction measurement was carried out at room temperature using an Agilent Gemini S diffractometer equipped with a CCD detector and molybdenum (Mo) radiation source. Acquired data were processed with the CrysAlisPro software [22]. Using Olex2 [23], the structure was solved with the olex2.solve [24] structure solution program using Charge Flipping and refined with the olex2.refine [24] refinement package using Gauss-Newton minimization. All non-hydrogen atoms were refined anisotropically, and hydrogen atoms were included in the model at calculated positions, refined with a rigid model with their Uiso value fixed at 1.2Ueq of their parent atoms.

Table 1 reports the crystallographic data and experimental details of data collection and structure refinements. Atomic coordinates and equivalent thermal parameters are reported in Table 2, selected bond distances in Table 3. The structural graphics were created using both DIAMOND program [25] and Mercury [26].

**Table 1.** Experimental X-ray data collection data collection details from  $(C_4N_2H_{14})[Co(H_2PO_3)_4] \cdot 2H_2O$ .

Chemical Formula	$(C_4N_2H_{14})[Co(H_2PO_3)_4] \cdot 2H_2O$
Mr (g/mol)	509.08
$F(000)$	263.9
Symmetry, S.G.	Triclinic (P-1, n. 2)
Cell parameters/V	A = 5.4814 (3) Å, b = 7.5515 (4) Å, c = 10.8548 (6) Å, $\alpha = 88.001 (4)^\circ$ , $\beta = 88.707 (5)^\circ$ , $\gamma = 85.126 (5)^\circ/447.33 (4) \text{ \AA}^3$
Z	1
$\lambda$ (Mo K $\alpha$ radiation) (Å)	0.71073
T(K)/ $\mu$ (mm $^{-1}$ )	298/1.39
Crystal sizes (mm)	0.25 × 0.25 × 0.3
Measured reflections/independent reflections (reflections with $I \geq 2\sigma(I)$ )/parameters	9480/2005 (1878)/137
$\theta_{\min} - \theta_{\max}$ ( $^\circ$ )/Rint	1.9–27.8/0.024
Reciprocal space limiting indices	h: –6–7, k: –9–9, l: –13–14
R[F $^2 > 2\sigma(F^2)$ ]/wR(F $^2$ )/G.O.F.	0.026/0.072/1.03

**Table 2.** Fractional atomic coordinates and displacement parameters (Å $^2$ ) for the atoms in  $(C_4N_2H_{14})[Co(H_2PO_3)_4] \cdot 2H_2O$  (“\*” isotropic parameters for H atoms).

	x	y	z	Uiso */Ueq
Co1	0.5	0	0.5	0.01218 (11)
P5	–0.02030 (8)	0.22049 (6)	0.42698 (4)	0.01422 (12)
H5	–0.007 (4)	0.111 (3)	0.344 (2)	0.021 (5) *
P7	0.52560 (9)	–0.06370 (6)	0.80899 (4)	0.01853 (13)
H7	0.634 (5)	–0.223 (3)	0.790 (2)	0.033 (6) *
O2	0.2188 (2)	–0.17568 (17)	0.48203 (12)	0.0186 (3)
O3	0.4308 (2)	0.01773 (18)	0.68967 (11)	0.0221 (3)
O4	0.2349 (2)	0.22465 (16)	0.47498 (12)	0.0183 (3)
O6	–0.0899 (3)	0.4083 (2)	0.36416 (14)	0.0276 (3)
H6	–0.234 (6)	0.439 (4)	0.365 (3)	0.051 (9) *
O8	0.6876 (3)	0.0461 (2)	0.87800 (13)	0.0335 (4)
O9	0.3019 (3)	–0.1124 (2)	0.89129 (13)	0.0346 (4)
H9	0.324 (2)	–0.087 (4)	0.9627 (5)	0.0519 (6) *
O13	–0.5521 (3)	0.5209 (2)	0.35642 (15)	0.0261 (3)
H13a	–0.574 (6)	0.602 (4)	0.387 (3)	0.044 (9) *
H13b	–0.607 (5)	0.442 (4)	0.388 (2)	0.030 (7) *
N12	0.0271 (3)	0.2595 (2)	0.77025 (14)	0.0220 (3)
H12a	–0.027 (2)	0.3488 (2)	0.7196 (6)	0.0264 (4) *
H12b	0.1433 (7)	0.1909 (15)	0.7321 (7)	0.0264 (4) *
H12c	–0.0966 (17)	0.1953 (15)	0.79227 (19)	0.0264 (4) *
C10	–0.0486 (4)	0.4687 (3)	0.94033 (18)	0.0263 (4)
H10a	–0.2031 (4)	0.4179 (3)	0.95693 (18)	0.0316 (5) *
H10b	–0.0785 (4)	0.5696 (3)	0.88336 (18)	0.0316 (5) *
C11	0.1294 (4)	0.3320 (3)	0.88205 (18)	0.0264 (4)
H11a	0.1693 (4)	0.2355 (3)	0.94144 (18)	0.0316 (5) *
H11b	0.2794 (4)	0.3857 (3)	0.85960 (18)	0.0316 (5) *

**Table 3.** Most relevant bond lengths (Å) and angles (°) from (C<sub>4</sub>N<sub>2</sub>H<sub>14</sub>)[Co(H<sub>2</sub>PO<sub>3</sub>)<sub>4</sub>].2H<sub>2</sub>O.

Co1—O2	2.1336 (12)	P5—O6	1.5732 (14)
Co1—O2i	2.1336 (12)	P7—O3	1.4987 (13)
Co1—O3	2.0919 (12)	P7—O8	1.4955 (15)
Co1—O3i	2.0919 (12)	P7—O9	1.5625 (15)
Co1—O4i	2.1519 (12)	N12—C11	1.489 (2)
Co1—O4	2.1519 (12)	C10—C10iii	1.517 (4)
P5—O2ii	1.5050 (13)	C10—C11	1.505 (3)
P5—O4	1.5067 (13)		
O2i—Co1—O2	180	O4—Co1—O3	87.41 (5)
O3i—Co1—O2	88.26 (5)	O4i—Co1—O4	180
O3—Co1—O2	91.74 (5)	O4—P5—O2ii	117.53 (7)
O3—Co1—O2i	88.26 (5)	O6—P5—O2ii	109.58 (8)
O3i—Co1—O2i	91.74 (5)	O6—P5—O4	106.61 (8)
O3i—Co1—O3	180	O8—P7—O3	115.59 (9)
O4—Co1—O2i	90.01 (5)	O9—P7—O3	108.23 (8)
O4—Co1—O2	89.99 (5)	O9—P7—O8	110.69 (8)
O4i—Co1—O2i	89.99 (5)	P5ii—O2—Co1	129.16 (7)
O4i—Co1—O2	90.01 (5)	P7—O3—Co1	139.61 (8)
O4i—Co1—O3i	87.41 (5)	P5—O4—Co1	126.28 (7)
O4i—Co1—O3	92.59 (5)	C10—C11—N12	111.66 (16)
O4—Co1—O3i	92.59 (5)		

Symmetry codes: (i)  $-x + 1, -y, -z + 1$ ; (ii)  $-x, -y, -z + 1$ ; (iii)  $-x, -y + 1, -z + 2$ .

Supplementary tables of crystal structure and refinement, notably the full list of bond lengths and angles, and anisotropic thermal parameters were deposited with the Inorganic Crystal Structure Database, FIZ, Hermann von Helmholtz Platz 1, 76344 EggensteinLeopoldshafen, Germany; fax: (+49) 7247 808 132; Email: crysdata@fiz-karlsruhe.de. Deposition number is CCDC 1882579.

## 2.4. Biological Activities

### 2.4.1. Nematicidal Activity

The model nematode *Steinernema feltiae* was purchased from Sautter und Stepper GmbH (Ammerbuch, Germany) in the form of powder and stored at 4 °C in the dark. Fresh samples were utilized prior to each experiment. A homogeneous mixture was prepared by dissolving 200 mg of nematode powder in 50 mL distilled water. Later on, the nematode suspension was placed for 15 min at room temperature with shaking and in moderate light. Viability was examined under a light microscope at four-fold magnification (TR 200, VWR International, Leuven, Belgium). The viability of nematodes above 80% in each sample was considered a prerequisite for each experiment. Ten microliters of nematode suspension were added to each well of a 96-well plate. The hybrid cobalt phosphite (C<sub>4</sub>N<sub>2</sub>H<sub>14</sub>)[Co(H<sub>2</sub>PO<sub>3</sub>)<sub>4</sub>].2H<sub>2</sub>O was then added into the wells to achieve final concentrations of 250, 500, and 1000 μM. Afterward, the final volume in each well was adjusted to 100 μL by adding Phosphate Buffered Saline (PBS pH = 7.4). PBS and ethanol (10 μL per well) were employed as negative and positive controls, respectively, and sterile distilled water was the solvent control. Each experiment was performed independently on three different occasions and in triplicate ( $n = 9$ ). Living and dead nematodes were counted under the microscope prior to treatment, and the viability fraction ( $V_0$ ) was calculated (usually >0.9). Then, 50 μL of lukewarm water (40 °C) was added to each well to stimulate the nematodes prior to counting. After 24 h, the  $V_{24}$  fraction was calculated, by once more counting the living and dead nematodes, and expressed as a percentage of initial viability  $V_0$  according to the equation:

$$\text{Viability (\%)} = [V_{24}/V_0] \times 100$$

Results are represented as mean ± SD, and GraphPad Prism (Version 5.03, GraphPad Software, La Jolla, CA, USA) was used to calculate the statistical significances by one-way ANOVA.  $p < 0.05$  was considered to be statistically significant.

### 2.4.2. The Antimicrobial Activity

This section may be divided by subheadings. It should provide a concise and precise description of the experimental results, their interpretation, as well as the experimental conclusions, that can be drawn. The activity of  $(C_4N_2H_{14})[Co(H_2PO_3)_4] \cdot 2H_2O$  compound against *Escherichia coli*, *Staphylococcus epidermidis*, *Candida albicans*, and *Saccharomyces cerevisiae* was investigated in routine microbial growth assays based on optical density and recorded in the form of growth curves. Fresh cultures of *S. epidermidis*, *E. coli*, *C. albicans*, and *S. cerevisiae* were prepared on bacterial tryptic soy broth, Luria-Bertani broth (LB), Sabouraud Dextrose Agar (SDA), and Yeast Peptone Dextrose (YPD) agar media, respectively. After 18–24 h of incubation, the microbial colonies from these Agar plates were then transferred into 10 mL solution of 0.9% *w/v* NaCl (saline), and the turbidity of the suspension was adjusted to 0.5 of McFarland standard. These microbial suspensions were then exposed to the samples as described below. Bacterial and yeast culture with growth medium were employed as negative control, sterile distilled water was utilized as solvent control, while the positive control consisted of a mixture of 10,000 units/mL of penicillin, 10,000  $\mu\text{g/mL}$  of streptomycin, and 25  $\mu\text{g/mL}$  of amphotericin B. The sample was evaluated at various dilutions (of 250, 500, and 1000  $\mu\text{M}$ ), and the plates were incubated at 37 °C for 24 h. Microbial growth was monitored by recording the optical density of the samples at 0 h and 24 h, using a Micro Plate Reader E800 at 593 nm. These absorbance values were converted into percentages and compared to the negative control whose absorbance values were normalized to 100% and served as references at each time interval. All experiments were carried out in triplicate at three different occasions ( $n = 9$ ). Results are represented as mean  $\pm$  SD, and statistical significances were calculated by one-way ANOVA using GraphPad Prism (Version 5.03, GraphPad Software, La Jolla, CA, USA) with  $p < 0.05$  considered to be of statistical significance.

## 3. Results and Discussion

### 3.1. Structural Description

As shown in Figure 1, there is one crystallographically distinct site for Co atom in the asymmetric unit of  $(C_4N_2H_{14})[Co(H_2PO_3)_4] \cdot 2H_2O$ , which contains 13 non-hydrogen atoms, including 2 oxygen atoms “O13” as water molecules. Cobalt cation shows octahedral geometry, coordinating six oxygen atoms from adjacent phosphite groups. The Co–O bond lengths range from 2.0920 (1) Å to 2.1336 (1) Å (Table 3), with an average Co–O distance of 2.1258 Å, in good agreement with the value 2.113 Å reported in  $[(C_4N_8H_{12})Co(HPO_3)_2(C_2O_4)_3]$  [27] and to that of 2.101 Å for  $NaCo(H_2PO_3)_3 \cdot H_2O$  [28]. All  $H_2PO_3^-$  units adopt pseudo-tetrahedral coordination geometry. P(5) shares two oxygen with adjacent Co atoms, while P(7)O4 tetrahedral group is connected by one P–O–Co bond and possesses a short terminal P–O bond (1.4945 (1) Å). The P–O bond distances are in the range 1.5050(13)–1.5732(14) Å for P(5) atom [Av. 1.5283 Å] and 1.4987(13)–1.5625(15) Å for P(7) [Av. 1.5189 Å]. P(5) and P(7) atoms have a terminal phosphite P–H bond 1.241 (1) and 1.3127 (1) Å, respectively. These values are in good agreement with those reported in  $(C_2NH_8)_2[Co_3(HPO_3)_4]$ ,  $(C_4N_2H_{12})[Co(HPO_3)_2]$  [29], and  $(C_6H_{16}N_2)[Co(HPO_3)F]$  [30]. The strict alternation of  $CoO_6$  octahedra and  $H_2PO_3^-$  pseudo pyramids via oxygen vertices results in an anionic network with a Co/P ratio of 1/2. The polyhedral units are joined through corners sharing four-membered rings, which are thereby connected through their edges forming an infinite one-dimensional chain rising along [100] (Figure 2). The individual chain units are further linked together through hydrogen bond interactions (Figure 3, Table 4). The 1,4-butanediammonium templates, which resides between the parallel chains, are diprotonated. They are further ensuring, together with the free-standing water molecules, the stability of the three-dimensional network.

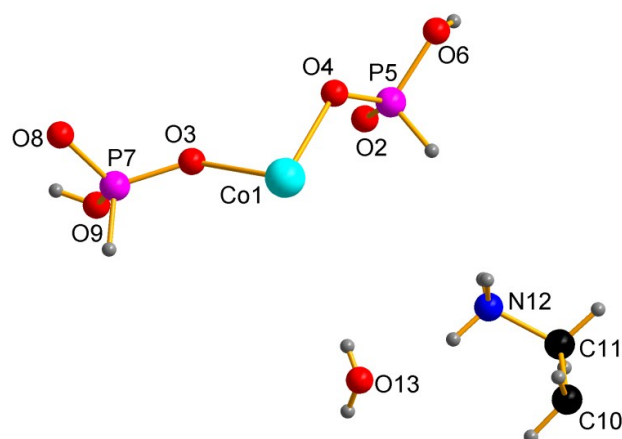


**Figure 1.** Asymmetric unit of  $(C_4N_2H_{14})[Co(H_2PO_3)_4] \cdot 2H_2O$ . Thermal ellipsoids are shown at 50% probability.

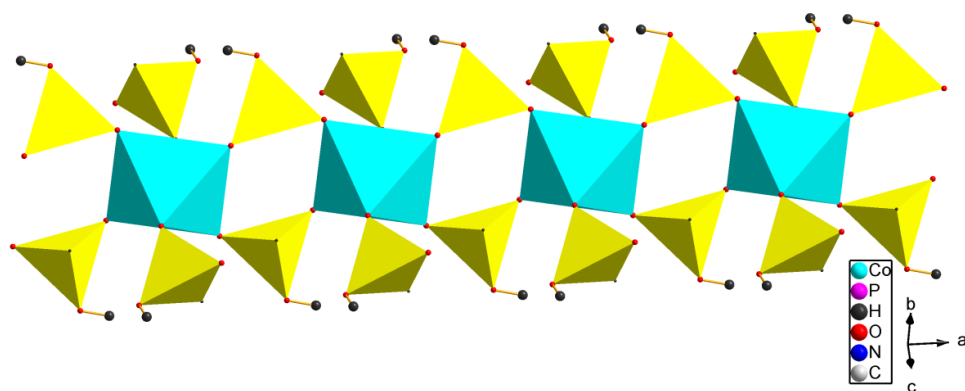


**Figure 2.** A fragment of the structure of  $(C_4N_2H_{14})[Co(H_2PO_3)_4] \cdot 2H_2O$  along  $[010]$ , showing the infinite four-membered ring chain propagating along  $[100]$ .

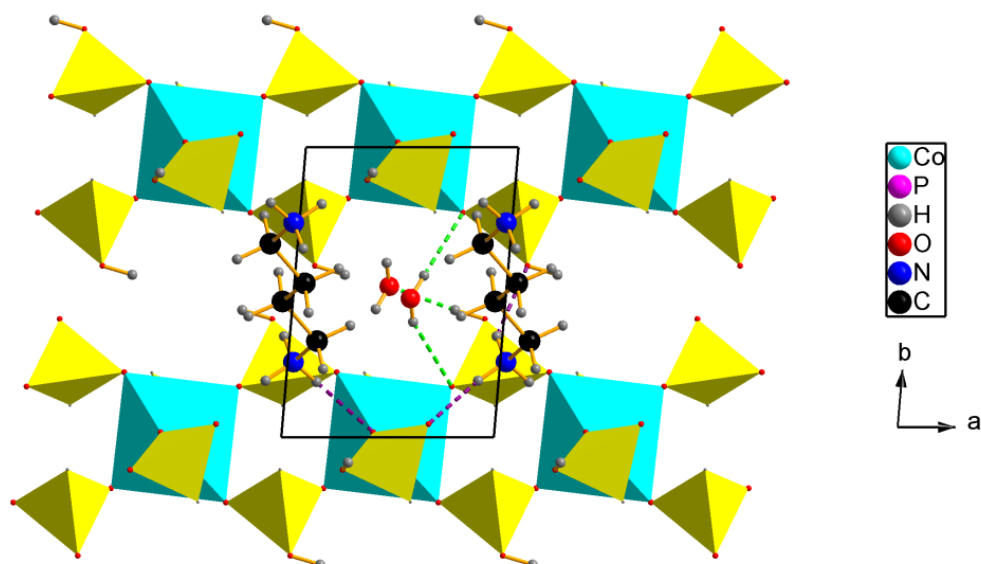


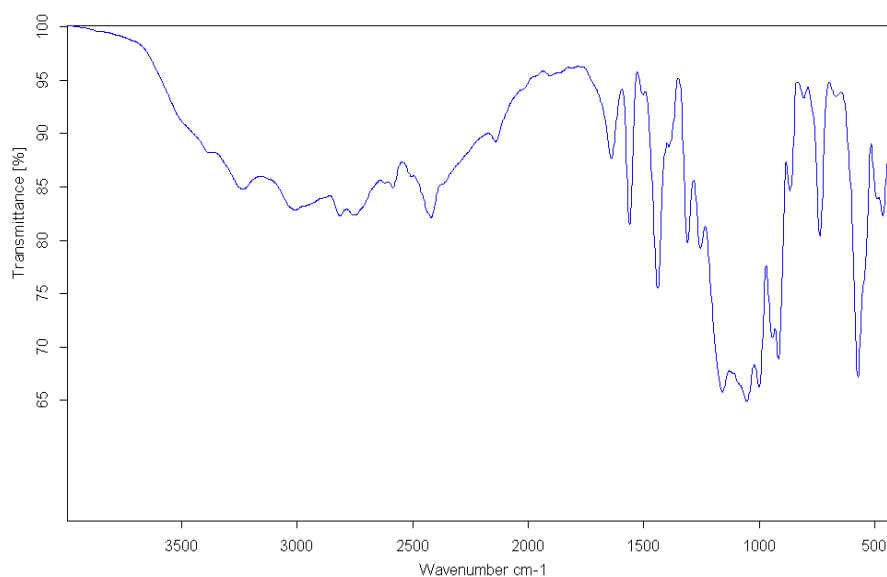
**Figure 3.** The crystal structure of  $(C_4N_2H_{14})[Co(H_2PO_3)_4] \cdot 2H_2O$  in a projection along  $c$ -axis emphasizing the hydrogen bonds (dashed lines).

**Table 4.** Hydrogen bonding network in the framework of  $(C_4N_2H_{14})[Co(H_2PO_3)_4] \cdot 2H_2O$ .

D-H...A	D-H/Å	H...A/Å	D...A/Å	DHA/°
O6-H6...O13	0.80 (3)	1.80 (3)	2.605 (2)	175 (3)
O9-H9...O8	0.82 (1)	1.77 (1)	2.574 (2)	169(1)
N12-H12A...O6	0.89 (1)	2.16 (1)	2.900 (2)	140 (1)
N12-H12B...O3	0.89 (1)	2.02 (1)	2.887 (2)	166 (1)
N12-H12C...O8	0.89 (1)	1.91 (1)	2.776 (2)	165 (1)
O13-H13A...O2	0.71 (3)	2.22 (3)	2.888 (2)	159 (3)
O13-H13B...O4	0.76 (3)	2.11 (3)	2.863 (2)	179 (4)

### 3.2. Infrared Spectroscopy

The infrared spectrum of  $(C_4N_2H_{14})[Co(H_2PO_3)_4] \cdot 2H_2O$  (Figure 4) exhibits bands corresponding to the vibration modes of the organic template and phosphite groups. The stretching vibration of  $NH_2$  in 1,4-butanediammonium cation is observed in the high frequencies  $3090\text{--}3200\text{ cm}^{-1}$ , while its bending appears at  $1600\text{ cm}^{-1}$  [31]. The values at around  $2850$  and  $1300\text{ cm}^{-1}$  are boil down to the stretching vibration of  $CH_2$  and  $C\text{--}N$ , respectively. The band appearing at  $2450\text{ cm}^{-1}$  corresponds to the stretching vibration of  $P\text{--}H$  bond which is the characteristic bond of phosphite groups, whereas the bands from  $990$  to  $1030\text{ cm}^{-1}$  are assigned to the bending mode of  $P\text{--}H$ . The vibration modes centered at  $570$ ,  $1050$ , and  $1160\text{ cm}^{-1}$  are ascribed to the stretching vibration of  $PO_3$  group, while the one located at  $910\text{ cm}^{-1}$  presents the stretching vibration of  $P\text{--}OH$  [20]. The set of bands related to the stretching vibration and deformation of the  $OH$  group belonging to water molecules is observed at around  $3000$  and  $1640\text{ cm}^{-1}$  [32,33].

**Figure 4.** The infrared spectrum of  $(C_4N_2H_{14})[Co(H_2PO_3)_4] \cdot 2H_2O$ .

### 3.3. Thermal Behavior

TGA experiment was performed under an air atmosphere. The experimental data, given from TG analysis (Figure 5), show three separated steps of weight loss in a total of 45% for  $(C_4N_2H_{14})[Co(H_2PO_3)_4] \cdot 2H_2O$ . The first mass loss of 10% in the range of  $180\text{--}220\text{ °C}$  is accompanied by an endothermic signal in the differential thermal analysis (DTA) trace at  $180\text{ °C}$ . The peak coincidences with the departure of 1.5 water molecules (calculated mass 9.8%). The second stage with a theoretical weight loss of 8% starting at about  $320\text{ °C}$  and ending at  $420\text{ °C}$  can be related to the decomposition of 1,4-butanediammonium (calculated weight loss 8%). This phenomenon is coupled with an exothermic heat flow noticed at  $340\text{ °C}$ . The total decomposition of the organic moiety and the remaining water

molecules is shown between 540–660 °C (observed weight loss 27%), with a small exothermic curve at 640 °C (calculated weight loss 27.8%).

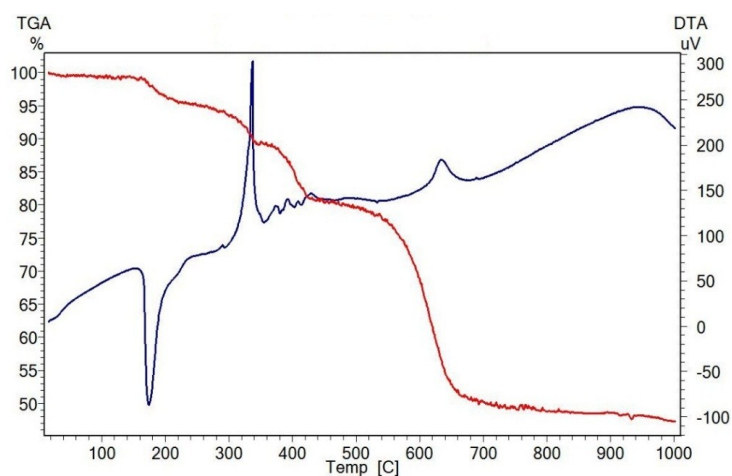


**Figure 5.** Thermogravimetric (TG) and differential thermal analysis (TDA) curves of  $(C_4N_2H_{14})[Co(H_2PO_3)_4] \cdot 2H_2O$ .

### 3.4. Biological Activities

The hybrid cobalt phosphite compound was tested for their antimicrobial activity against two bacterial (*Escherichia coli* and *Staphylococcus epidermidis*) and two fungal (*Saccharomyces cerevisiae* and *Candida albicans*) strains. The mixture of 10,000 units/mL of penicillin, 10,000  $\mu\text{g/mL}$  of streptomycin, and 25  $\mu\text{g/mL}$  of Amphotericin B was used as control drugs. The percentage inhibition and minimum inhibitory concentration (MIC) values of the compound based on the growth of microorganisms are shown in Figure 6a. The highest inhibition activity of the compound was observed against *C. albicans* fungi with a MIC value of 500  $\mu\text{g}\cdot\text{mL}^{-1}$ . The compound showed a lower activity against *E. coli* (1000  $\mu\text{g}\cdot\text{mL}^{-1}$ ) than positive control, while no significant activity was observed against *S. cerevisiae* and *S. epidermidis* strains.



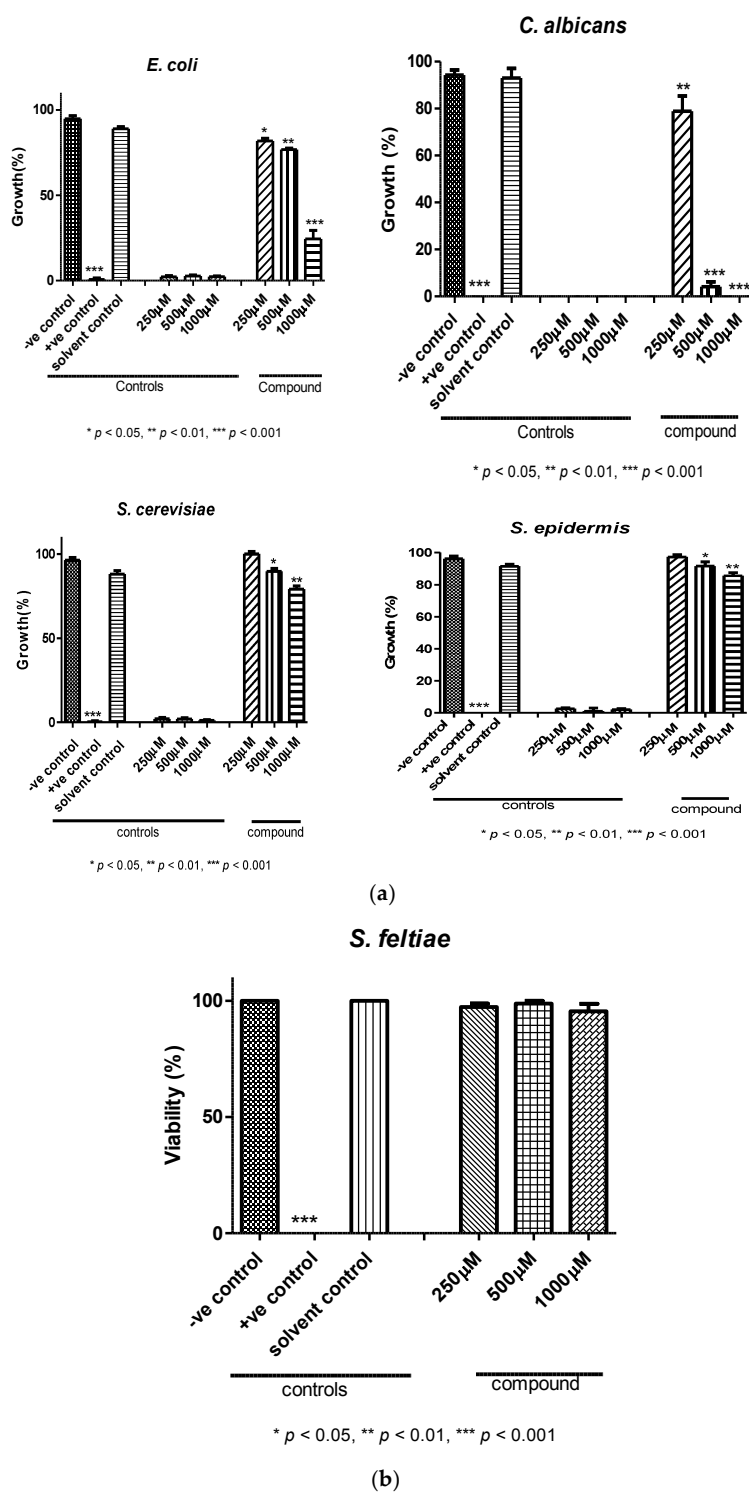


**Figure 6.** Antibacterial activity of  $(C_4N_2H_{14})[Co(H_2PO_3)_4] \cdot 2H_2O$  against bacterial and fungal strains (a) and *S. feltiae* nematode (b).

The nematicidal activity of  $(C_4N_2H_{14})[Co(H_2PO_3)_4] \cdot 2H_2O$  was investigated against *S. feltiae* nematode. Ethanol was used as a positive control. No mortality of nematodes was observed; such a result indicates that the hybrid compound was inactive against *S. feltiae* (Figure 6b).

#### 4. Conclusions

New organically templated cobalt phosphite  $(C_4N_2H_{14})[Co(H_2PO_3)_4] \cdot 2H_2O$  has been synthesized using wet chemistry. Single crystal structure analysis revealed that the framework displays a chain-like structure, containing vertex sharing four-membered rings formed by the connectivity between  $CoO_6$  octahedrons and  $H_2PO_3^-$  pseudo-tetrahedral units bound through their edges. The diprotonated 1,4-butanediammonium acts as a stabilizer of the inorganic network through hydrogen bonds. The thermogravimetric analysis showed that the dehydration of the hybrid phosphite takes place in three steps, resulting mainly from the loss of the organic moiety and water molecules. The antimicrobial investigation showed significant activity against some microorganisms, that is, *C. albicans* and almost no activity against *S. feltiae*, suggesting that the activity of the compound is related to the type of the studied microorganisms.

**Author Contributions:** N.H. performed the experiments and started writing the manuscript as part of her thesis report, S.C. supported her under the supervision of M.L. I.d.S. solved the crystal structure. M.E. measured the thermal features of the material, R.A., A.Y.A. and C.J. achieved the biological tests and wrote the corresponding part of the manuscript. B.E.B. planned the research, rewrote the crystal structure part and finalized writing the manuscript.

**Funding:** This research had no external funding.

**Acknowledgments:** The authors would like to acknowledge the support and technical assistance of Interface Regional University Center (Sidi Mohammed Ben Abdellah University, Fez) and National Center for Scientific and Technical Research (CNRST-Rabat). Alhasan would like to acknowledge Dahye Kim and Hyemin Oh from Ewha Womans University (South Korea) for their participation in the biological activities tests.

**Conflicts of Interest:** The authors declare no conflict of interest.

#### References

1. Garcia-Fernandez, A.; Bermudez-Garcia, J.M.; Castro-Garcia, S.; Artiaga, R.; Lopez-Beceiro, J.; Senaris-Rodriguez, M.A.; Sanchez-Andujar, M. Dielectric properties induced by the framework in the hybrid organic-inorganic compounds  $M(dca)_2pyz$   $M = Fe, Co$  and  $Zn$ . *Polyhedron* **2016**, *114*, 249–255. [[CrossRef](#)]
2. Xiong, D.B.; Li, M.R.; Liu, W.; Chen, H.H.; Yang, X.X.; Zhao, J.T. Synthesis, structure and luminescence property of two lanthanum phosphite hydrates:  $La_2(H_2O)_x(HPO_3)_3$  ( $x = 1, 2$ ). *J. Solid State Chem.* **2006**, *179*, 2571–2577. [[CrossRef](#)]
3. Wang, L.; Song, T.; Fan, Y.; Tian, Z.; Wang, Y.; Shi, S.; Xu, J. Synthesis and characterization of a new open-framework fluorinated gallium phosphite with three-dimensional intersecting channels. *J. Solid State Chem.* **2006**, *179*, 3400–3405. [[CrossRef](#)]
4. Chung, U.C.; Mesa, J.L.; Pizarro, J.L.; Jubera, V.; Lezama, L.; Arriortua, M.I.; Rojo, T.  $Mn(HPO_3)_2$ : A new manganese (II) phosphite with a condensed structure. *J. Solid State Chem.* **2005**, *178*, 2913–2921. [[CrossRef](#)]
5. Shi, S.H.; Qian, W.; Li, G.H.; Wang, L.; Yuan, H.M.; Xu, J.N.; Zhu, G.S.; Song, T.Y.; Qiu, S.L. Building three-dimensional metal phosphites from the corner-shared four-membered rings chain. *J. Solid State Chem.* **2004**, *177*, 3038–3044.
6. Lin, Z.E.; Fan, W.; Gao, F.; Chino, N.; Yokoi, T.; Okubo, T. A novel layered bimetallic phosphite intercalating with organic amines: Synthesis and characterization of  $Co(H_2O)_4Zn_4(HPO_3)_6 \cdot C_2N_2H_{10}$ . *J. Solid State Chem.* **2006**, *179*, 723–728. [[CrossRef](#)]
7. Zhong, Y.J.; Chen, Y.M.; Sun, Y.Q.; Yang, G.Y. Syntheses and characterization of two new zinc phosphites with 1D chains decorated by Zn-centered complexes. *J. Solid State Chem.* **2005**, *178*, 2613–2619. [[CrossRef](#)]
8. Agarwal, R.A.; Mukherjee, S. One dimensional coordination polymers of Cd(II) and Zn(II): Synthesis, structure, polar packing through strong inter-chain hydrogen bonding and gas adsorption studies. *Polyhedron* **2016**, *106*, 163–170. [[CrossRef](#)]
9. Ouarsal, R.; Tahiri, A.A.; El Bali, B.; Lachkar, M.; Bolte, M. Strontium dihydrogenphosphite. *Acta Crystallogr.* **2002**, *E58*, i19–i20. [[CrossRef](#)]
10. Ouarsal, R.; Tahiri, A.A.; Lachkar, M.; Slimani, Z.; El Bali, B.; Bolte, M. Barium dihydrogen phosphate hemihydrates. *Acta Crystallogr.* **2002**, *E58*, i72–i73.

11. Chaouche, S.; Ouarsal, R.; El Bali, B.; Lachkar, M.; Bolte, M.; Dusek, M.  $\text{Li}_2\text{HPO}_3 \cdot \text{H}_2\text{O}$ : Crystal Structure and IR Spectrum. *J. Chem Crystallogr.* **2010**, *40*, 526–530. [[CrossRef](#)]
12. El Bali, B.; Massa, W. Redetermination of copper(II) hydrogenphosphite dehydrate. *Acta Crystallogr.* **2002**, *E58*, i29–i31.
13. Chaouch, S.; Ouarsal, R.; Akouibaa, M.; Rakib, S.; Lachkar, M.; El Bali, B.; Dusek, M.  $\text{Cs}_2[\text{M}(\text{H}_2\text{O})_6]_3(\text{HPO}_3)_4$ ,  $\text{M} = \text{Co}, \text{Ni}$ : Crystal structures, IR and thermal studies. *J. Phys. Conf. Ser.* **2018**, *984*, 12–15. [[CrossRef](#)]
14. Ouarsal, R.; Tahiri, A.A.; El Bali, B.; Lachkar, M.; Harrison, W.T.A. Sodium zinc tris(dihydrogenphosphite) hydrate  $\text{NaZn}(\text{H}_2\text{PO}_3)_3 \cdot \text{H}_2\text{O}$ . *Acta Crystallogr.* **2002**, *E58*, i23–i25. [[CrossRef](#)]
15. Ouarsal, R.; Tahiri, A.A.; Lachkar, M.; Dusek, M.; Fejfarová, K.; El Bali, B. Sodium magnesium tris(dihydrogenphosphite)monohydratehydrate,  $\text{NaMg}(\text{H}_2\text{PO}_3)_3 \cdot \text{H}_2\text{O}$ . *Acta Crystallogr.* **2003**, *E59*, i33–i35.
16. Ouarsal, R.; Essehli, R.; Lachkar, M.; Zenkouar, M.; Dusek, M.; Fejfarová, K.; El Bali, B. Dipotassium cobalt(II) bis(hydrogenphosphite) dihydrate,  $\text{K}_2\text{Co}(\text{HPO}_3)_2 \cdot 2\text{H}_2\text{O}$ . *Acta Crystallogr.* **2004**, *E60*, i66–i68.
17. Messouri, I.; El Bali, B.; Capitelli, F.; Piniella, J.F.; Lachkar, M.; Slimani, Z. Diammoniumtris [hexaaquamagnesium(II)]tetrakis[hydrogenphosphate(III)],  $(\text{NH}_4)_2[\text{Mg}(\text{H}_2\text{O})_6]_3(\text{HPO}_3)_4$ . *Acta Crystallogr.* **2005**, *E61*, i129–i131.
18. Ouarsal, R.; El Bali, B.; Lachkar, M.; Dusek, M.; Fejfarová, K. Diammoniumtris [hexaaquanickel(II)] tetrakis[hydrogenphosphate(III)],  $(\text{NH}_4)_2[\text{Ni}(\text{H}_2\text{O})_6]_3(\text{HPO}_3)_4$ . *Acta Crystallogr.* **2005**, *E61*, i171–i173.
19. Ouarsal, R.; El Bali, B.; Lachkar, M.; Dusek, M.; Fejfarová, K. Diammonium tris[hexaaquacobalt(II)] tetrakis[hydrogenphosphate(III)],  $(\text{NH}_4)_2[\text{Co}(\text{H}_2\text{O})_6]_3(\text{HPO}_3)_4$ . *Acta Crystallogr.* **2005**, *E61*, i168–i170. [[CrossRef](#)]
20. Ouarsal, R.; Lachkar, M.; Dusek, M.; Albert, E.B.; Castelló, J.B.C.; El Bali, B. Crystal structure of  $\text{NaCd}(\text{H}_2\text{PO}_3)_3 \cdot \text{H}_2\text{O}$  and spectroscopic study of  $\text{NaM}(\text{H}_2\text{PO}_3)_3 \cdot \text{H}_2\text{O}$ ,  $\text{M} = \text{Mn}, \text{Co}, \text{Ni}, \text{Zn}, \text{Mg}$  and  $\text{Cd}$ . *Polyhedron.* **2016**, *106*, 132–137. [[CrossRef](#)]
21. Chaouche, S.; Ouarsal, R.; Lachkar, M.; Capitelli, F.; El Bali, B. Crystal Structure and IR Study of  $(\text{C}_6\text{H}_5\text{NH}_3)[\text{ZnCl}(\text{HPO}_3)]$ . *J. Chem Crystallogr.* **2010**, *40*, 486–490. [[CrossRef](#)]
22. *CrysAlisPro Software System*, Version 1.171.38.41; Rigaku Corporation: Oxford, UK, 2015.
23. Dolomanov, O.V.; Bourhis, L.J.; Gildea, R.J.; Howard, J.A.K.; Puschmann, H. OLEX2: A complete structure solution, refinement and analysis program. *J. Appl. Cryst.* **2009**, *42*, 339–341. [[CrossRef](#)]
24. Bourhis, L.J.; Dolomanov, O.V.; Gildea, R.J.; Howard, J.A.K.; Puschmann, H. The anatomy of a comprehensive constrained, restrained refinement program for the modern computing environment—*Olex2* dissected. *Acta Cryst. A* **2015**, *71*, 59–75. [[CrossRef](#)] [[PubMed](#)]
25. Brandenburg, K.; Putz, H. *DIAMOND Version 3*; Crystal Impact GbR: Bonn, Germany, 2005.
26. Macrae, C.F.; Bruno, I.J.; Chisholm, J.A.; Edgington, P.R.; McCabe, P.; Pidcock, E.; Rodriguez-Monge, L.; Taylor, R.; Van de Streek, J.; Wood, P.A. Mercury CSD 2.0—New Features for the Visualization and Investigation of Crystal Structures. *J. Appl. Cryst.* **2008**, *41*, 466–470. [[CrossRef](#)]
27. Mandal, S.; Natarajan, S. Inorganic–organic hybrid structure: Synthesis, structure and magnetic properties of a cobalt phosphite–oxalate,  $[\text{C}_4\text{N}_2\text{H}_{12}][\text{Co}_4(\text{HPO}_3)_2(\text{C}_2\text{O}_4)_3]$ . *J. Solid State Chem.* **2005**, *178*, 2376–2382. [[CrossRef](#)]
28. Kratochvíl, B.; Podlahova, J.; Habibpur, S.; Petricek, V.; Maly, K. Cobalt(II) sodium dihydrogenphosphite monohydrate. *Acta Cryst.* **1982**, *B38*, 2436–2438. [[CrossRef](#)]
29. Liu, X.; Xing, Y.; Liu, X. Solvothermal synthesis and magnetic properties of cobalt(II) phosphite structures of varying dimensionality. *Cryst. Eng. Commun.* **2010**, *12*, 383–386. [[CrossRef](#)]
30. Fernández-Armas, S.; Mesa, J.L.; Pizarro, J.L.; Chung, U.C.; Arriortua, M.I.; Rojo, T. Two new two-dimensional organically templated phosphite compounds:  $(\text{C}_6\text{H}_{16}\text{N}_2)_{0.5}[\text{M}(\text{HPO}_3)\text{F}]$ ,  $\text{M} = \text{Fe}(\text{II})$  and  $\text{Co}(\text{II})$ : Solvothermal synthesis, crystal structures, thermal, spectroscopic, and magnetic properties. *J. Solid State Chem.* **2005**, *178*, 3554–3562. [[CrossRef](#)]

31. Kantarcı, Z.; Sag lam, S.; Kasap, E. Vibrational spectroscopic studies on the 1,4-diaminobutane- $T_d$ -type clathrates:  $Cd(dabn)M(CN)_4 \cdot 1,5C_6H_6$  ( $M = Cd$  or  $Hg$ ). *Spectrosc. Lett.* **2002**, *35*, 811–819. [[CrossRef](#)]
32. Novak, A. Hydrogen bonding in solids correlation of spectroscopic and crystallographic data. In *Large Molecules. Structure and Bonding*; Springer: Berlin/Heidelberg, Germany, 1974; pp. 177–216.
33. Gilli, G.; Gilli, P. Towards a Unified Hydrogen-Bond Theory. *J. Mol. Struct.* **2000**, *552*, 1–15. [[CrossRef](#)]



© 2019 by the authors. Licensee MDPI, Basel, Switzerland. This article is an open access article distributed under the terms and conditions of the Creative Commons Attribution (CC BY) license (<http://creativecommons.org/licenses/by/4.0/>).